Electronic Supplementary Material (ESI) for Energy & Environmental Science.
This journal is © The Royal Society of Chemistry 2020

Electronic Supplementary Information

Discovery of high-performance thermoelectric copper chalcogenide using modified diffusion-couple high-throughput synthesis and automated histogram analysis technique

Tingting Deng, [abc] Tong Xing, [ab] Madison Brod, [d] Ye Sheng, [e] Pengfei Qiu,*[ab] Igor Veremchuk, [f] Qingfeng Song, [ab] Tian-Ran Wei, [g] Jiong Yang, [ae] G. Jeffrey Snyder,*[d] Yuri Grin, [h] Lidong Chen [ab] and Xun Shi*[a]

a. State Key Laboratory of High Performance Ceramics and Superfine Microstructure, Shanghai Institute of Ceramics, Chinese Academy of Sciences, Shanghai 200050, China. E-mail: xshi@mail.sic.ac.cn, qiupf@mail.sic.ac.cn
b. Center of Materials Science and Optoelectronics Engineering, University of Chinese Academy of Sciences, Beijing 100049, China.
c. School of Physical Science and Technology, Shanghai Tech University, Shanghai 201210, China.
d. Department of Materials Science and Engineering, Northwestern University, Evanston, Illinois 60208, USA. E-mail: jeff.snyder@northwestern.edu
e. Materials Genome Institute, Shanghai University, Shanghai 200444, China.
f. Helmholtz-Zentrum Dresden-Rossendorf, Institute of Ion Beam Physics and Materials Research, 01328 Dresden, Germany.
g. State Key Laboratory of Metal Matrix Composites, School of Materials Science and Engineering, Shanghai Jiao Tong University, Shanghai 200240, China.
h. Max-Planck-Institut für Chemische Physik fester Stoffe, Dresden, Germany.

Lattice dynamics calculations

Lattice dynamics were obtained by Density-Functional Theory (DFT) calculations with Vienna ab initio simulation package (VASP)[1, 2], using the frozen phonon method which is implemented in the Phonopy package. The projector-augmented wave (PAW) method as implemented in the Perdew−Burke−Ernzerhof (PBE)-type generalized gradient approximation (GGA) was used as the exchange−correlation functional[3]. Based on the crystallographic information obtained by the X-ray refinement (model 2), we firstly built an order 2 × 2 × 2 supercell of Cu_3SnS_4. Then, two Cu atoms in the

supercell are replaced by Sn atoms to form the chemical composition ($Cu_{22}Sn_{10}S_{32}$) that is close to $Cu_7Sn_3S_{10}$ based on special quasirandom structures (SQS's) calculations.[4] The plane-wave energy cutoff was set at 450 eV and a 3× 3 × 3 Monkhorst-Pack k mesh was used for crystal structure optimization to realize the convergence of Hellmann–Feynman forces. It is adopted that convergence criteria of 5×10^{-5} eV/Å for relaxation process of unit cell and 5×10^{-7} eV/Å for static calculation of displaced supercell at gamma point in accurate precision. The spin-orbit coupling (SOC) effect has not been considered.

Table S1 Crystallographic information of $Cu_7Sn_3S_{10}$ prepared by melting-annealing-ball milling method (model 1). Here the composition is normalized to 16 atoms in the unit cell.

Composition	$Cu_{6.28}Sn_{1.72}S_{8.00}$
Formula weight	859.77
Space group	*I*2*m* (No. 121)
a /Å	5.4163(3)
c /Å	10.833(1)
Unit cell volume /Å^3	317.79(7)
F (000) /e	396.1
Z	1
μ/cm^{-1}	502.62
Calculated density (g cm^{-3})	4.492(1)
Radiation, wavelength(Å)	Cu*K*α, 1.54056
T (K)	295
Data range 2θ (°)	10 - 110
No. of reflections	152
No. of refined structure parameters	7
Profile function	Pseudo-Voigt

Refinement mode	Full profile
R_i	0.0393
R_p	0.0720
R_{wp}	0.0489
Goodness of fit	1.850

Table S2 Crystallographic information of $Cu_7Sn_3S_{10}$ prepared by melting-annealing-ball milling method (model 3). Here the composition is normalized to 16 atoms in the unit cell.

Composition	$Cu_{5.56(2)}Sn_{2.33(4)}S_{8.10(2)}$
Formula weight	890.3
Space group	*I*2*m* (No. 121)
a /Å	5.4162(2)
c /Å	10.8335(7)
Unit cell volume /Å^3	317.80(5)
F (000) /e	407.5
Z	1
μ/cm^{-1}	589.3
Calculated density (g cm^{-3})	4.65
Radiation, wavelength(Å)	Cu *K*α, 1.54056
T (K)	295
Data range 2θ (°)	10 - 110
No. of reflections	152
No. of refined structure parameters	7
Profile function	Pseudo-Voigt
Refinement mode	Full profile
R_i	0.032
R_p	0.050
R_{wp}	0.067
Goodness of fit	1.76

Table S3 Selected Bond Lengths (Å) and Angles (°) for $Cu_7Sn_3S_{10}$ in the model 2.

Cu1-S1	2.319(7)		
Cu2-S1	2.334(4)		
Cu3-S1	2.334(4)		
S1-Cu1-a S1 7)	111.86(2)	a S1-Cu2-b S1 7) [0010]	109.58(2)
S1-Cu1-b S1 7) [0000]	104.78(2)	a S1-Cu2-c S1	109.25(2)
S1-Cu1-c S1 7) [0000]	111.86(2)	b S1-Cu2-c S1	109.58(2)
a S1-Cu1-b S1 7) [0000]	111.86(2)	S1-Cu3-a S1 6)	111.99(2)
a S1-Cu1-c S1	104.78(2)	S1-Cu3-a S1 6) [0010]	108.23(2)
b S1-Cu1-c S1	111.86(2)	S1-Cu3-c S1 6) [0000]	108.23(2)
S1-Cu2-a S1 7)	109.58(2)	a S1-Cu3-b S1 6) [0-100]	108.23(2)
S1-Cu2-b S1 7) [0100]	109.25(2)	a S1-Cu3-c S1	108.23(2)
S1-Cu2-c S1 7) [0110]	109.58(2)	b S1-Cu3-c S1	111.99(2)

Symmetry codes: (1) x, y, z; (2) -y, x, -z; (3) -x, -y, z; (4) y, -x, -z; (5) -x, y, -z; (6) y, x, z; (7) x, -y, -z; (8) -y, -x, z; (9) 1/2+x, 1/2+y, 1/2+z ; (10) 1/2-y , 1/2+x , 1/2-z ; (11) 1/2-x, 1/2-y, 1/2+z ; (12) 1/2+y , 1/2-x , 1/2-z ; (13) 1/2-x, 1/2+y, 1/2-z ; (14) 1/2+y, 1/2+x, 1/2+z ; (15) 1/2+x , 1/2-y , 1/2-z ; (16) 1/2-y , 1/2-x, 1/2+z.

Table S4 Parameters used to fit the heat capacity (C_p) data of $Cu_7Sn_3S_{10}$ by using a Debye and two Einstein modes. The Debye temperature (Θ_D) is derived by the equation $\Theta_D = (12\pi^4 N k_B/5\beta)^{1/3}$.

Fitting parameters	**One Debye + one Einstein**
ϕ (10^{-4} J mol^{-1} K^{-2})	6.90
β (10^{-5} J mol^{-1} K^{-4})	9.32
A (J mol^{-1} K^{-1})	2.94
Θ_E (K)	83.13
Θ_D (K)	275
R^2	0.99997
χ^2	0.000000126

Table S5 Parameters used to fit the lattice thermal conductivity of $Cu_7Sn_3S_{10}$.

Fitting parameters	$Cu_7Sn_3S_{10}$
L (μm)	0.53
A (10^{-41} s^3)	0.603
B (10^{-18} s K^{-1})	11.265
C (10^{36} s^{-3})	4.541
ω/v (THz)	10.9/1.73
R^2	0.99828
χ^2	0.02738

*ω is angular frequency and v is frequency, and their units are the same THz. (i.e. $\omega=2\pi v$)

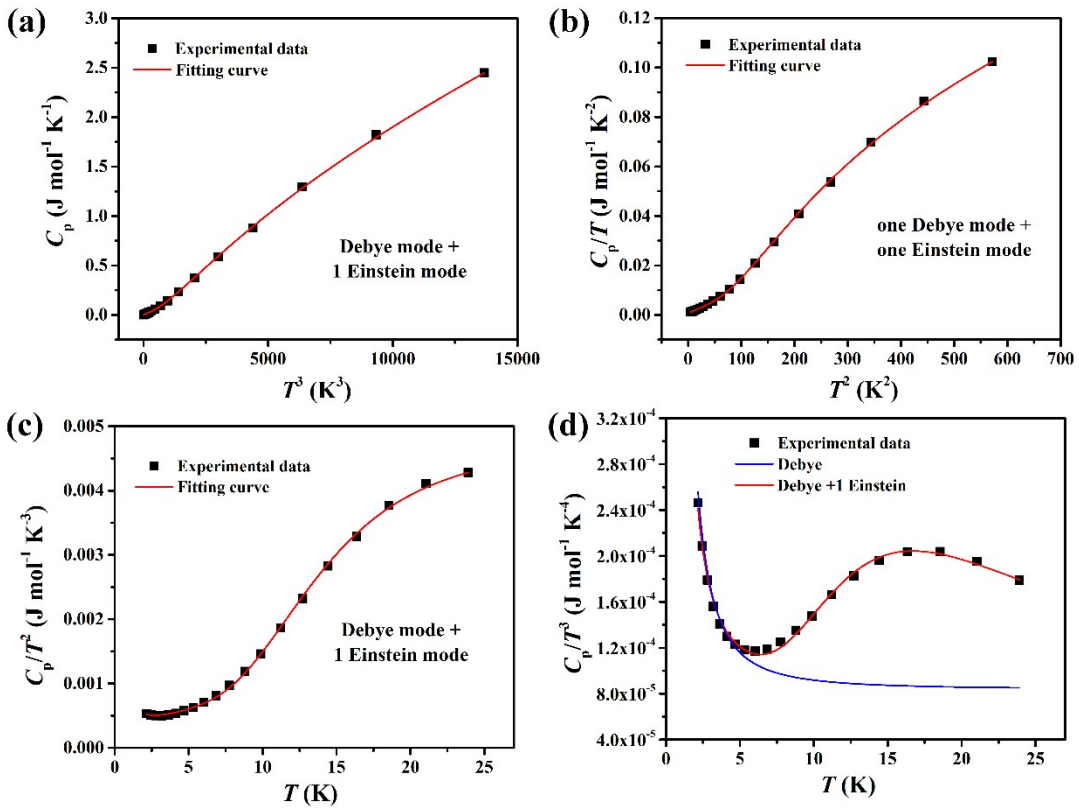

Fig. S1 Heat capacity fitting for $Cu_7Sn_3S_{10}$ from 2 to 25 K. (a-c) C_p versus T^3, C_p/T versus T^2, and C_p/T^2 versus T for $Cu_7Sn_3S_{10}$ by using one Debye mode + one Einstein mode. (d) C_p/T^3 versus T for $Cu_7Sn_3S_{10}$ from 2 K to 25 K fitted by Debye mode and one Debye mode + one Einstein mode, respectively.

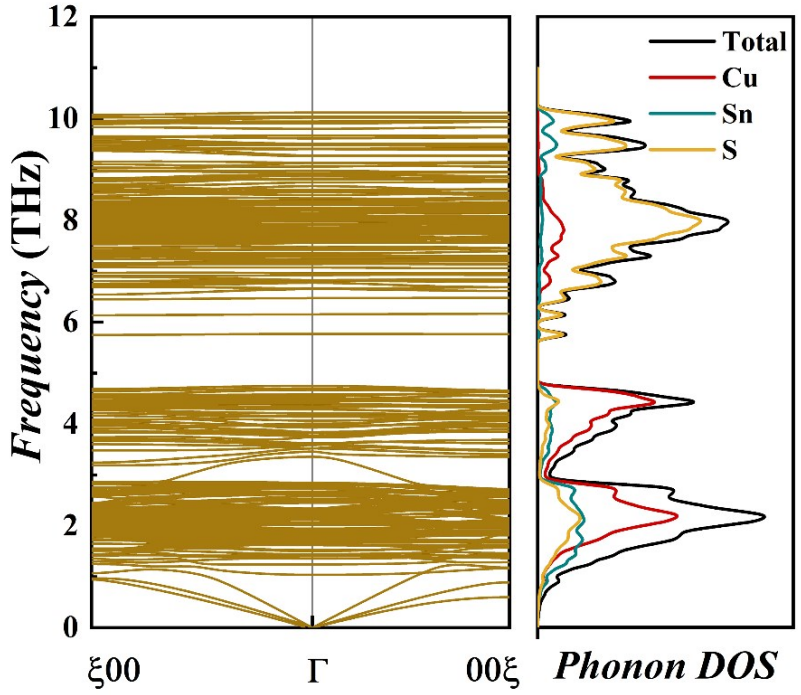

Fig. S2 Phonon dispersions and projected phonon density of states for $Cu_7Sn_3S_{10}$.

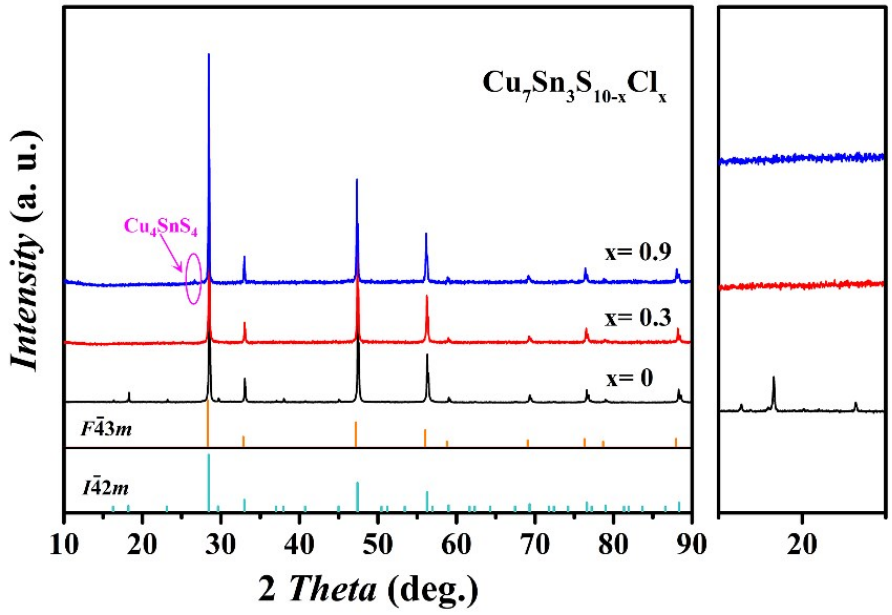

Fig. S3 Powder X-ray diffraction patterns for $Cu_7Sn_3S_{10-x}Cl_x$ (x=0, 0.3, and 0.9) samples. The appearance of diffraction peaks belonging Cu_4SnS_4 indicates that the Cl-doping content in $Cu_7Sn_3S_{10}$ is less than x = 0.9.

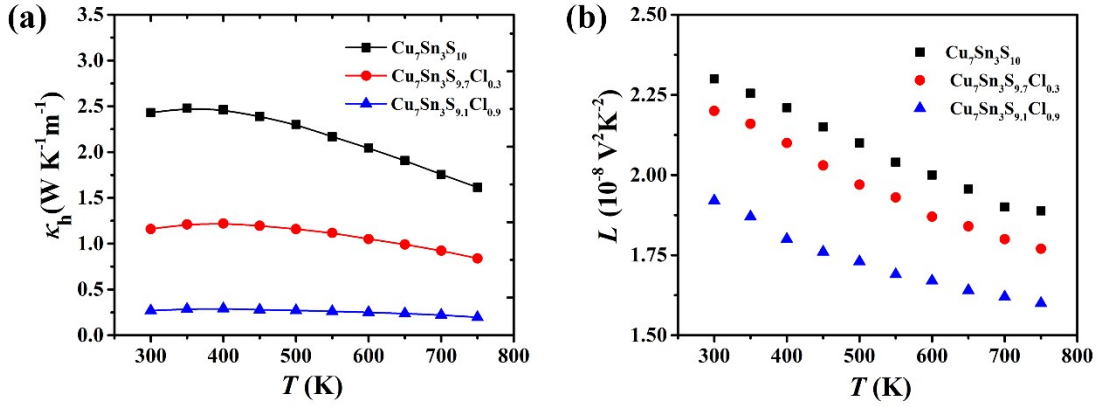

Fig. S4 Carrier thermal conductivity (κ_h) and Lorenz number (L) derived by the single parabolic band model for $Cu_7Sn_3S_{10}$, $Cu_7Sn_3S_{9.7}Cl_{0.3}$, and $Cu_7Sn_3S_{9.1}Cl_{0.9}$ samples from 300 K to 750 K.

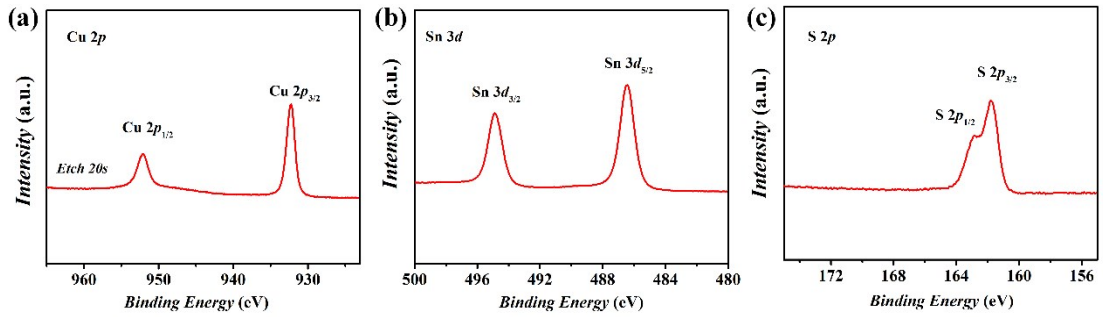

Fig. S5 XPS spectra of $Cu_7Sn_3S_{10}$: (a) Cu 2p, (b) Sn 3d, and (c) S 2p.

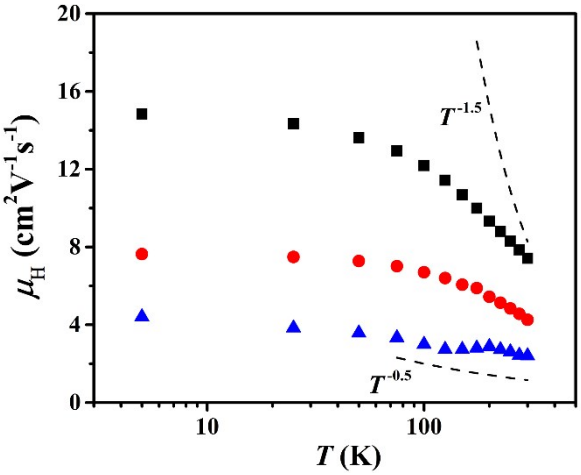

Fig. S6 Temperature dependence of Hall carrier mobility (μ_H) for $Cu_7Sn_3S_{10-x}Cl_x$ (x=0, 0.3, and 0.9) samples from 5 K to 300 K. The dashed lines represent the μ_H-$T^{-1.5}$ and μ_H-$T^{-0.5}$ relationships, respectively.

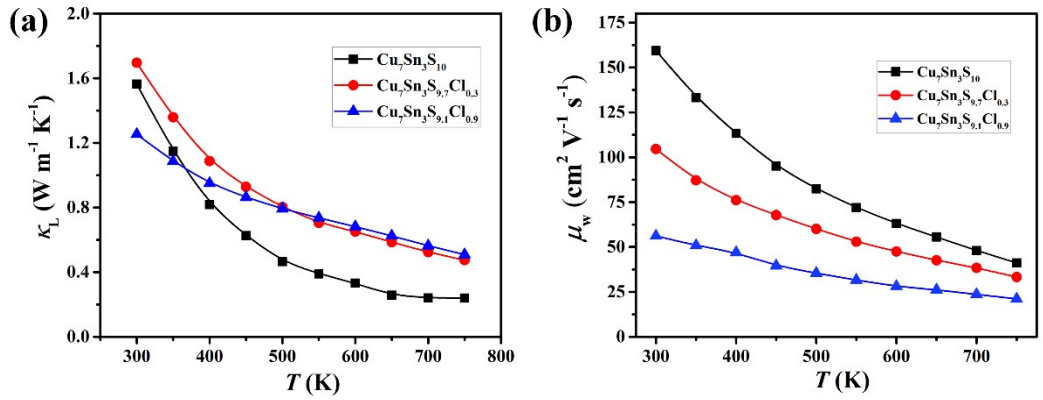

Fig. S7 (a) Lattice thermal conductivity κ_L as a function of temperature for $Cu_7Sn_3S_{10-x}Cl_x$. It decreases with temperature as expected from phonon-phonon scattering and is not strongly influenced by the Cl content. (b) The weighted mobility μ_w as a function of temperature for $Cu_7Sn_3S_{10-x}Cl_x$. It decreases with temperature as expected from phonon scattering and decreases with Cl content.

References

1. G. Kresse and J. Furthmu¨ller, *Phys. Rev. B*, 1996, **54**, 11169-11186.
2. P. E. Blochl, *Phys. Rev. B*, 1994, **50**, 17953-17979.
3. J. P. Perdew, K. Burke and M. Ernzerhof, *Phys. Rev. Lett.*, 1996, **77**, 3865-3868.
4. A. van de Walle, P. Tiwary, M. de Jong, D. L. Olmsted, M. Asta, A. Dick, D. Shin, Y. Wang, L. Q. Chen and Z. K. Liu, *Calphad*, 2013, **42**, 13-18.